Electronic Research Archive

http://www.aimspress.com/journal/era

ERA, 32(6): 4108–4128.
DOI: 10.3934/era.2024185
Received: 30 December 2023
Revised: 29 May 2024
Accepted: 12 June 2024
Published: 26 June 2024

Research article

The important role of astrocytes in activity pattern transition of the subthalamopallidal network related to Parkinson's disease

Yuzhi Zhao[1,2], **Honghui Zhang**[1,2,*] **and Zilu Cao**[1,2]

[1] School of Mathematics and Statistics, Northwestern Polytechnical University, Xi'an 710129, China
[2] MIIT Key Laboratory of Dynamics and Control of Complex Systems, Xi'an 710129, China

* **Correspondence:** Email: haozhucy@nwpu.edu.cn.

Abstract: This paper integrates astrocytes into the subthalamopallodal network model associated with Parkinson's disease (PD) to simulate the firing activity of this circuit. Under different network connectivity modes, we primarily investigate the role of astrocytes in the discharge rhythm of the subthalamic nucleus (STN) and the external segment of the globus pallidus (GPe). First, with varying synaptic coupling, the STN-GPe model generates five typical waveforms corresponding to the severity of PD symptoms in a sparsely coupled network in turn. Subsequently, astrocytes are included in the STN-GPe circuit. When they have an inhibitory effect on the STN and an excitatory effect on the GPe, the pathological discharge pattern of the network can be destroyed or even eliminated under appropriate conditions. At the same time, the high degree of synchrony between neurons and the power of the beta band weakens. In addition, we find that the astrocytic effect on the GPe plays a dominant role in the regulatory process. Finally, the tightly coupled network can also generate five different, highly correlated sustained discharge waveforms, including in-phase and anti-phase cluster synchronization. The effective regulation of the pathological state of PD, which involves improvements in the discharge patterns, synchronization, and beta oscillations, is achieved when astrocytes inhibit the STN and excite the GPe. It is worth noting that the regulatory influence of astrocytes on PD is shown to be robust, and independent of the network connectivity, to some extent. This work contributes to understanding the role of astrocytes in PD, providing insights for the treatment and regulation of PD.

Keywords: Parkinson's disease; subthalamopallidal network; astrocyte

1. Introduction

Parkinson's disease (PD) is a common degenerative disease of the nervous system. The physiological trigger is mainly the degeneration and death of dopaminergic neurons in the substantia nigra pars compacta, though the exact cause is still unclear [1]. The mechanism is relatively complex; therefore,

the study of the pathological mechanism and clinical control of PD are key scientific issues in related fields at home and abroad.

The dynamic characterization of PD mainly reflects the discharge mode. Specifically, there is a significant increase in the proportion of cluster discharges in action potentials of neurons in the PD state, as well as an increased synchrony between adjacent neurons [2]. In the normal state, neurons discharge randomly, showing a chaotic state, and usually do not produce cluster discharge behavior, which is closely related to the severity of the disease in PD patients. In addition, an analysis of local field potential signals recorded by deep brain stimulation (DBS) electrodes in PD patients found that the relative power in the beta frequency band (13–30 Hz) in PD patients was higher than in the normal state [3]. Unit neuron activity and local field potentials recorded from the basal ganglia of PD animals and patients showed changes in oscillatory behaviors that could interfere with information processing in the basal ganglia and cause motor dysfunction.

Current dynamic models of PD are mainly limited to neuronal populations and rarely consider astrocytes. However, increasing evidence suggests that astrocytes play an important role in numerous neurodegenerative diseases, such as PD [4–6]. Astrocytes are the most abundant cells in the central nervous system (CNS) and are involved in maintaining the physiological functions of the CNS. When the body is stimulated, microglia are the first to activate, secrete pro-inflammatory factors, and act on astrocytes. Astrocytes amplify the inflammatory response mediated by microglia and release more pro-inflammatory factors, thus forming a vicious feedback loop. Activated astrocytes not only aggravate the amplification of inflammatory signals, but also produce glutamate and oxidative stress products, thus mediating the death of dopaminergic neurons [7]. Moreover, astrocytes promote the establishment and maturation of synaptic structures by releasing a variety of factors, while enhancing synaptic transmission by regulating the distribution of glutamate receptors. In addition, they can participate in the elimination of synapses through direct and indirect mechanisms [8]. Moreover, recent studies have highlighted the impact of astrocytes on neuronal circuits and synaptic functions in PD [9–12]. Iovino et al. suggested that any neuroprotective loss of astrocytes or gains in neurotoxic phenotypes could lead to glutamate-mediated PD toxicity [5]. Brandebura et al. pointed out that astrocytes are key players in PD, which is characterized by altered synaptic function, synaptic loss, and neuronal death [13]. Theoretical research on the involvement of glial cells in disease models has begun to emerge [14]. Among them, highly simplified astrocyte models, such as the "tripartite synapse", have achieved accuracy and predictability of ion concentration dynamics such as calcium, sodium, and potassium [15–17]. Mathematical modeling of the interaction mechanisms between neurons and astrocytes suggested that astrocytes could contribute to the generation of epileptiform discharges by directly affecting the excitatory/inhibitory balance of neuronal networks [18]. However, few studies have considered the mechanism of astrocyte involvement in PD from a theoretical perspective. Employing dynamic modeling helps reveal the role of astrocytes in PD circuits, thus offering comprehensive insights into the mechanisms and potential therapeutic avenues for PD.

Inspired by these findings, this paper focuses on investigating the influence of astrocytes on the PD-related neural circuit (i.e., the subthalamic nucleus - globus pallidus (STN-GPe) model). Sections 2–4 provide a dynamical description of the proposed model, the main results, and the conclusions and discussions, respectively.

2. Models

2.1. Description of the STN-GPe network

The STN-GPe model plays a vital pacemaker role in the basal ganglia, which is highly correlated with the generation of PD-associated discharge patterns. Therefore, we will adopt the model proposed in [19]. It can simulate a variety of discharge waveforms, some of which correspond to the synchronous oscillatory activity patterns observed in patients with PD, which are thought to be associated with symptoms of hypokinesia [20, 21]. Below is a brief description of the equations for each population [19]:

$$C_m v'_{STN} = -I_L - I_{Na} - I_K - I_T - I_{Ca} - I_{AHP} - I_{GPe\to STN}, \tag{2.1}$$

$$C_m v'_{GPe} = -I_L - I_{Na} - I_K - I_T - I_{Ca} - I_{AHP} - I_{STN\to GPe} - I_{GPe\to GPe} + I_{app}. \tag{2.2}$$

Here, $C_m = 1pF/\mu m^2$. I_L, I_{Na}, and I_K are the leak, sodium, and potassium ion currents, respectively. The current I_T is a low-threshold T-type calcium current. I_{Ca} is a high-threshold calcium current. I_{AHP} is a Ca^{2+}-activated, voltage-independent afterhyperpolarization K^+ current. $I_{GPe\to STN}$ represents the synaptic current from the GPe to the STN, which is similar to $I_{STN\to GPe}$ and $I_{GPe\to GPe}$. I_{app} is a constant bias current. For more details, please refer to the reference [19].

2.2. Description of the astrocyte model

Currently, some classical models have been proposed to simulate the dynamics of the intracellular Ca^{2+} concentration, among which the Li-Rinzel model is more commonly used, which can be expressed by the following equations:

$$\frac{d[Ca^{2+}]}{dt} = J_{chan} - J_{pump} + J_{leak}, \tag{2.3}$$

$$\frac{dq}{dt} = \alpha_q(1-q) - \beta_q q, \tag{2.4}$$

$$J_{chan} = c_1 v_1 p_\infty^3 n_\infty^3 q^3([Ca^{2+}]_{ER} - [Ca^{2+}]), \tag{2.5}$$

$$J_{pump} = \frac{v_3[Ca^{2+}]^2}{[Ca^{2+}]^2 + k_3^2}, \tag{2.6}$$

$$J_{leak} = c_1 v_2([Ca^{2+}]_{ER} - [Ca^{2+}]), \tag{2.7}$$

$$p_\infty = \frac{[IP_3]}{[IP_3] + d_1}, \tag{2.8}$$

$$n_\infty = \frac{[Ca^{2+}]}{[Ca^{2+}] + d_4}, \tag{2.9}$$

$$\alpha_q = a_1 d_2 \frac{[IP_3] + d_1}{[IP_3] + d_3}, \tag{2.10}$$

$$\beta_q = a_1[Ca^{2+}], \tag{2.11}$$

$$[Ca^{2+}]_{ER} = \frac{c_0 - [Ca^{2+}]}{c_1}, \tag{2.12}$$

where $[Ca^{2+}]$ denotes the cytosolic calcium concentration that varies in the time domain, and q is the fraction of activated IP3 receptors. J_{chan}, J_{pump}, and J_{leak} are the endoplasmic reticulum (ER)-to-cytosol calcium flux, the cytoplasm-to-ER pump flux, and the ER-to-cytosol leakage flux, respectively. $[Ca^{2+}]_{ER}$ is the calcium ion concentration in the ER. p_∞ and n_∞ are the calcium channel gated activation variables dependent on the IP3 concentration and the calcium ion concentration, respectively. α_q and β_q refer the activation and inactivation rates of the IP3 receptor channels, respectively. $[IP_3]$ indicates the production of intracellular IP3 in the astrocyte, which is modeled by the following:

$$\frac{d[IP_3]}{dt} = \frac{[IP_3^*] - [IP_3]}{\tau_{ip3}} + r_{ip3}([T]_{STN} + [T]_{GPe}), \tag{2.13}$$

where $[IP_3^*]$ is the equilibrium concentration of IP3. τ_{ip3} refers to a decay in the intracellular IP3 concentration. The parameter r_{ip3} determines the rate of IP3 production in response to a neuronal action potential. $[T]_{STN}/[T]_{GPe}$ represents the concentration of neurotransmitters released from the STN/GPe neuron to the synaptic cleft.

Table 1. Parameter value of astrocyte model.

Symbol	Value	Symbol	Value
$[Ca^{2+}]_{th}$	0.2 μM	v_1	6 s^{-1}
$\tau_{Ca^{2+}}$	6 s	v_2	0.11 s^{-1}
τ_{ip_3}	7 s	v_3	0.9 μMs^{-1}
r_{ip_3}	7.2 μMs^{-1}	d_1	0.13 μM
$[IP_3^*]$	0.16 μM	d_2	1.05 μM
c_0	2 μM	d_3	0.94 μM
c_1	0.185	d_4	0.082 μM
k_3	0.1 μM	k	0.5 s^{-1}
a_1	0.2 μM^{-1} s^{-1}		

Referring to the work of Volman et al. [22], the dynamic variable f is used to capture the interaction between neurons and astrocytes. Specifically, when the calcium concentration in the astrocytes exceeds a threshold value, a limited number of glial transmitters are released into the synaptic space, which in turn affects the excitability of the neighboring neurons. This interaction occurs through glutamate binding to presynaptic metabotropic glutamate (mGlu) and N-methyl-D-aspartate (NMDA) receptors. Because the source of neurotransmitters inside astrocytes is limited, the kinetic equation for f contains a saturation term $(1 - f)$. Therefore, the interaction between astrocytes and neurons can be expressed by the following formula [23–27]:

$$\frac{df}{dt} = \frac{-f}{\tau_{Ca^{2+}}} + (1 - f)k\phi([Ca^{2+}] - [Ca^{2+}]_{th}), \tag{2.14}$$

$$I_{STN}^{ast} = -\gamma_1 f, \tag{2.15}$$

$$I_{GPe}^{ast} = \gamma_2 f, \tag{2.16}$$

where $[Ca^{2+}]_{th}$ is the given calcium threshold, ϕ is the Heaviside step function, and k is the scaling factor. I_{STN}^{ast} and I_{GPe}^{ast} denote the currents of the astrocyte acting onto the STN and GPe, respectively,

and γ_1 and γ_2 are the functioning intensities of astrocyte. For specific parameter values, please refer to [24].

In addition, if we consider the effects of astrocytes on the STN and GPe neurons, then Eqs (2.1) and (2.2) will become the following:

$$C_m v'_{STN} = -I_L - I_{Na} - I_K - I_T - I_{Ca} - I_{AHP} - I_{GPe\to STN} - I^{ast}_{STN}, \tag{2.17}$$

$$C_m v'_{GPe} = -I_L - I_{Na} - I_K - I_T - I_{Ca} - I_{AHP} - I_{STN\to GPe} - I_{GPe\to GPe} - I^{ast}_{GPe} + I_{app}. \tag{2.18}$$

All simulations are written and performed under the MATLAB environment (The Mathworks, Natick, MA, USA). Ordinary differential equations in our system are integrated using the standard forward Euler method with a fixed temporal resolution of 0.01 ms. The total duration of the numerical simulation is set to $5 * 10^4$ ms.

3. Results

3.1. Sparsely connected circuit without astrocytes

Using the sparsely connected circuit described in [19], we can produce a variety of firing patterns as shown in Figure 1. Each STN sends an excitatory input to its nearest GPe neuron, while each GPe neuron sends an inhibitory input to the two directly adjacent GPe neurons and two STN neurons that skip the three nearest located STN neurons.

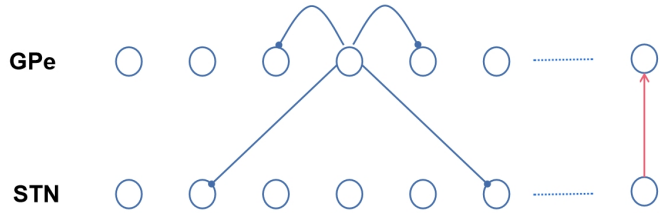

Figure 1. Schematic diagram of sparsely connected circuit of 10 STN neurons and 10 GPe neurons. Each STN sends excitatory input to its nearest GPe neuron, while each GPe neuron has inhibitory connections to the two directly adjacent GPe neurons and two STN neurons that skip the three nearest located neurons. The blue lines represent inhibitory connections and the red lines represent excitatory connections.

When the inhibitory effect of the GPe neurons is large, the STN may produce a rebound burst firing behavior. The stronger the inhibitory effect, the more obvious the rebound burst discharge of the STN, thus indicating that the pathological oscillation of PD is more serious. By changing the synaptic connection parameters between the STN and the GPe, we reproduce the five typical asynchronous discharge patterns in Figure 2.

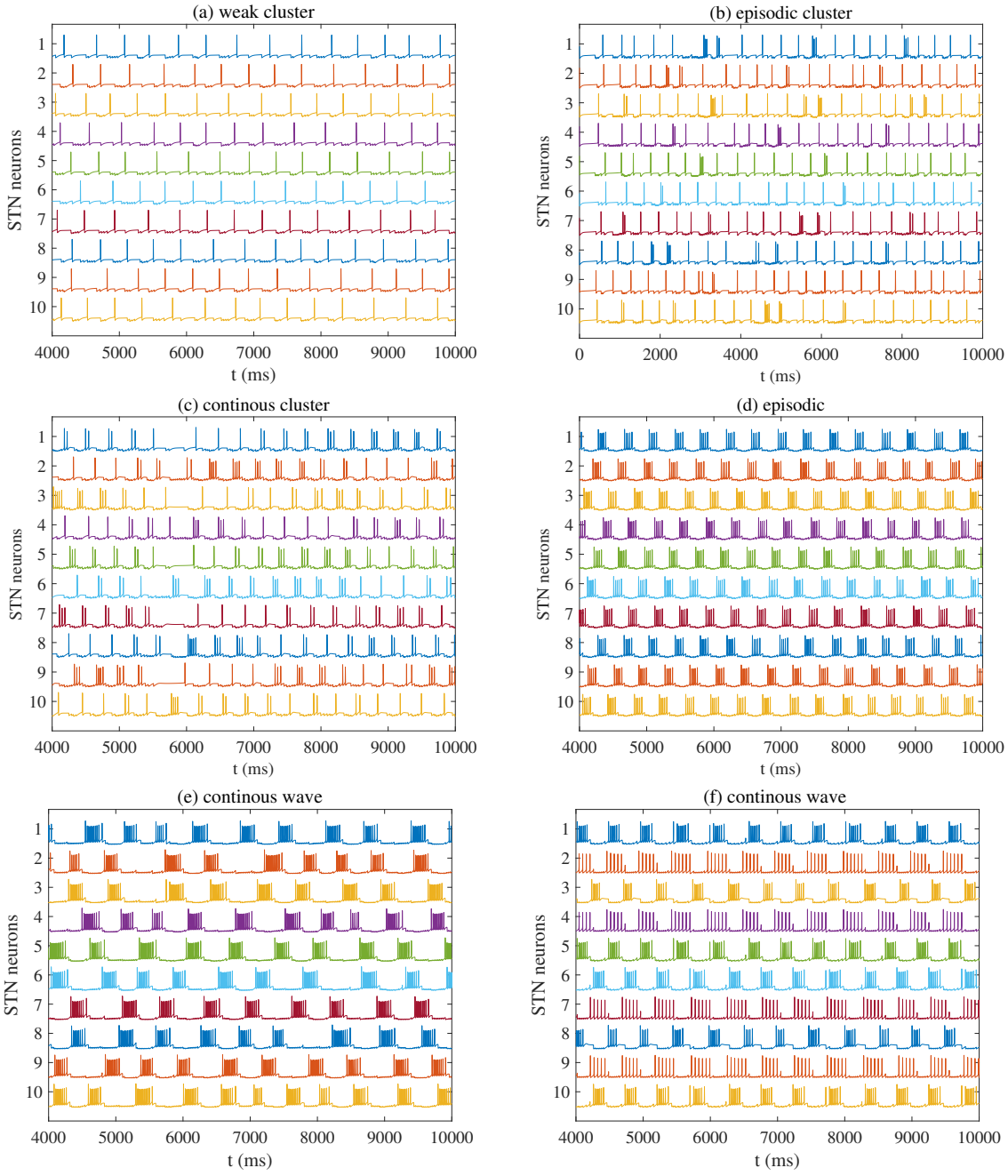

Figure 2. The activity patterns of STN neuron in the sparsely connected network. Five distinct firing patterns can be obtained by changing the values of synaptic parameters. (a) $g_{STN\to GPe} = 0.2\ nS/\mu m^2$, $g_{GPe\to STN} = 2.25\ nS/\mu m^2$. (b) $g_{STN\to GPe} = 0.6\ nS/\mu m^2$, $g_{GPe\to STN} = 2.25\ nS/\mu m^2$. (c) $g_{STN\to GPe} = 0.9\ nS/\mu m^2$, $g_{GPe\to STN} = 2.25\ nS/\mu m^2$. (d) $g_{STN\to GPe} = 0.9\ nS/\mu m^2$, $g_{GPe\to STN} = 2.5\ nS/\mu m^2$. (e) $g_{STN\to GPe} = 0.9\ nS/\mu m^2$, $g_{GPe\to STN} = 4.5\ nS/\mu m^2$. (f) $g_{STN\to GPe} = 0.9\ nS/\mu m^2$, $g_{GPe\to STN} = 4.5\ nS/\mu m^2$, select a set of initial values to make continous wave have significant inter-group/intra-group synchronization.

Here, we set the striatum input current $I_{app} = -1\ pA/\mu m^2$ for the GPe. As shown in Figure 2(a), when $g_{STN\to GPe} = 0.2\ nS/\mu m^2$, $g_{GPe\to STN} = 2.25\ nS/\mu m^2$, the STN exhibits a regular physiologi-

cal sparse firing, which is defined as a weak cluster. After strengthening the synaptic connection of the STN to the GPe, i.e., $g_{STN\to GPe} = 0.6\ nS/\mu m^2$, $g_{GPe\to STN} = 2.25\ nS/\mu m^2$ (see Figure 2(b)), the excitation of the GPe leads to an increased inhibition of STN, such that some random burst firings appear in the STN, and this discharge pattern is named as an episodic cluster. When $g_{STN\to GPe}$ to $0.9\ nS/\mu m^2$, $g_{GPe\to STN} = 2.25\ nS/\mu m^2$ (see Figure 2(c)) continuously increases, the discharge mode of the STN changes to a continuous cluster. Then, we fix $g_{STN\to GPe} = 0.9\ nS/\mu m^2$. In Figure 2(d), when $g_{GPe\to STN} = 2.5\ nS/\mu m^2$, the STN shows a continuous burst discharge behavior, which is defined as episodic. With $g_{GPe\to STN} = 4.5\ nS/\mu m^2$, the STN's rebound burst lasts longer and we define it as a continuous wave. Considering that excessive beta-band oscillations (13–30 Hz) and a high synchronization between the STN neuron firing are closely related to the severity of PD symptoms, we select two groups of different initial values to obtain a continous wave discharge pattern and take it as the initial pathological state in the simulation below. As shown in Figure 2(f), we can capture the obvious in-phase and anti-phase firings between the two groups.

It is worth noting that five discharge modes are generated in the sparsely connected network, in which a weak cluster, an episodic cluster, and a continuous cluster indicate healthy physiological states. In contrast, episodic and continuous waves indicate pathological oscillations of the PD state.

3.2. Sparsely connected circuit with astrocytes

Then, we further consider the role of astrocytes on the sparsely connected STN-GPe network, as shown in Figure 3. For simplicity, this subsection assumes that astrocytes have the same regulatory effect on the STN and the GPe (i.e., $\gamma_1 = \gamma_2 = \gamma$). When γ takes a negative value, it means that the astrocytes have an inhibitory effect on the STN and an excitatory effect on the GPe. Note that the minus sign here is only to indicate the ultimate excitatory/inhibitory effect of the astrocytes on the neurons, and does not indicate the magnitude of the coupling strength γ. The initial pathological selection of continuous waves with an obvious synchronicity as shown in Figure 2(f), and at t = $0.5 * 10^4$ ms, we change the value of γ from 0 to -2.3, -4, -6, and -7, respectively. As seen in Figure 4, we can clearly see the waveform transitions after the astrocytes act on neurons. When changing the coupling strength from -2.3 to -7, weak clusters, episodic clusters, continuous clusters, and episodic can all arise under appropriate conditions, and become out of synchronization. Specifically, in Figure 4(a), when γ is -2.3, the astrocytes gradually modulate pathological wave discharge and arise sporadic sparse firing, breaking the synchronous discharge of the STN. When γ increases to -4 (see Figure 4(b)), the corresponding firing alternately transforms into weak cluster and episdic cluster alternately. By increasing coupling strength to -6 (see Figure 4(c)), the discharge mode of the STN is nearly in weak cluster. As displayed in Figure 4(d)), with a larger coupling strength of -7, the STN are suppressed, resulting in sparse firing. Figure 4 demonstrates that the astrocytes acting on neurons can modulate the pathological firing pattern of the STN.

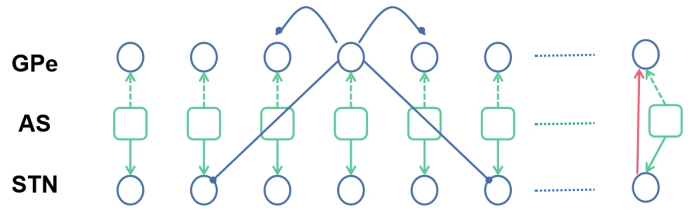

Figure 3. Schematic diagram of sparsely connected circuit of STN-GPe-AS (astrocytes). The connection between STN-GPe is the same as that shown in Figure 1. Each astrocyte acts on the adjacent STN and GPe. The blue lines represent inhibitory connections and the red lines represent excitatory connections. Solid and dotted lines in green indicate the effects of astrocytes on STN and GPe respectively.

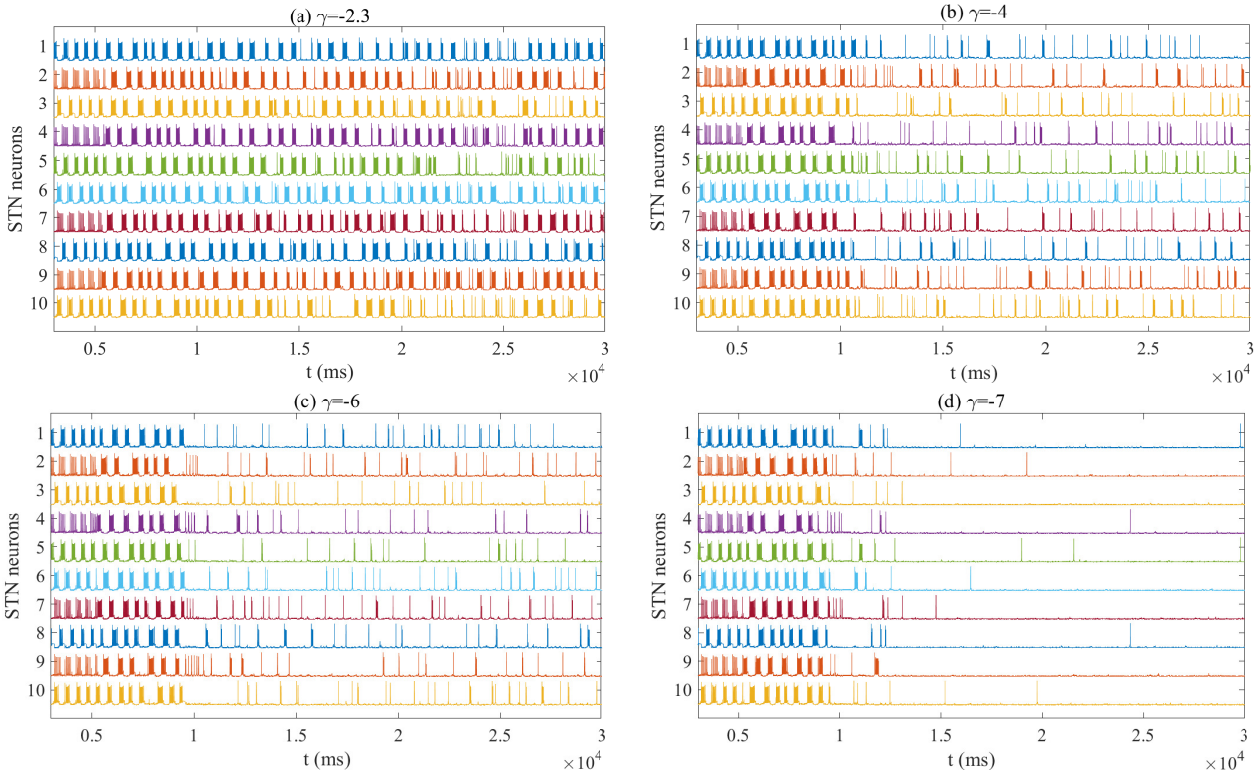

Figure 4. The response of STN population under different coupling strength γ. (a) $\gamma = -2.3$. (b) $\gamma = -4$. (c) $\gamma = -6$. (d) $\gamma = -7$. Note that the minus sign here is only to indicate the ultimate excitatory/inhibitory effect of the astrocytes on the neurons, and does not indicate the magnitude of the coupling strength γ (similarly hereinafter). The initial pathological selection of continuous waves with obvious synchronicity as shown in Figure 2(f). Under appropriate coupling strength γ, weak clusters, episodic clusters, continuous clusters, episodic and continuous waves can originate, and remain out of synchronous all the time.

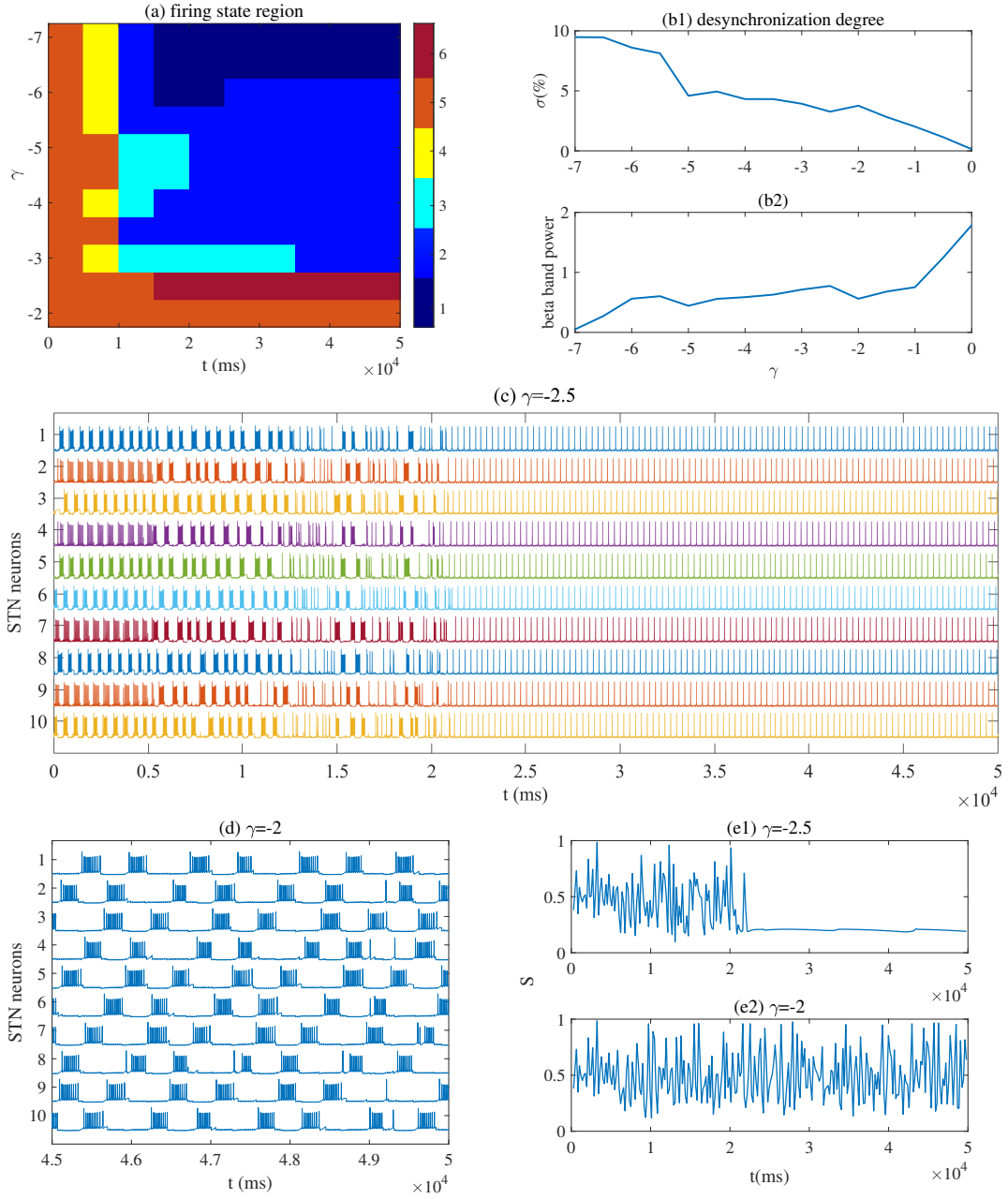

Figure 5. (a) Firing state transitions diagram. (b1, b2) The relationship between the two dynamical measures (i.e., desynchronization degree and the beta band power) and γ. (c, d) STN population patterns under coupling strength $\gamma = -2.5$ and $\gamma = -2$ respectively. (e1, e2) STN's synchronization degree S in case of (c, d).

To more systematically investigate the effect of the coupling strength γ, we vary the value of γ from -7 to 0. Based on the above phenomenon, we provide the firing state transition diagram of the STN, as shown in Figure 5(a). Due to the very rapid and transient nature of STN evolution, achieving precise firing state distinctions based on time series is challenging. Consequently, while our method of determining the discharge patterns shown here is not definitive, it can still provide meaningful insights into the role of astrocytes. From the perspective of temporal evolution, when the γ value exceeds

-2.5, the firing state of the STN neurons is more likely to transition from a pathological mode to a more sparse episodic cluster firing pattern. In addition, [28–30] used the variance of neuronal voltage to define the degree of desynchronization and thus quantitatively measured the synchrony between neurons. When the voltage activity of neurons is synchronized, their voltage waveforms have similar shapes and frequencies, resulting in a lower variance of the neuronal voltage. On the contrary, when the voltage activity of neurons is asynchronous, their voltage waveforms greatly differ, resulting in a higher variance of neuronal voltage. Therefore, using the variance of neuronal voltage to represent the desynchronization degree is an intuitive and effective method, which can help us quantify the degree of synchronization of neuronal networks. The specific formula is as follows:

$$\sigma = \frac{1}{T}\sum_{j=1}^{T}\sqrt{\sigma(j)}, \tag{3.1}$$

$$\sigma(j) = \frac{1}{N}\sum_{i=1}^{N}[V(j)^i]^2 - \frac{1}{N}(\sum_{i=1}^{N}[V(j)^i])^2, \tag{3.2}$$

where i and j represent the indexes of neurons and time steps, respectively. In total, there are 10 STN neurons (N = 10) and the total numerical simulation time is $5 * 10^4$ ms. When the desynchronization index is larger, it means that the synchronization of the system is lower.

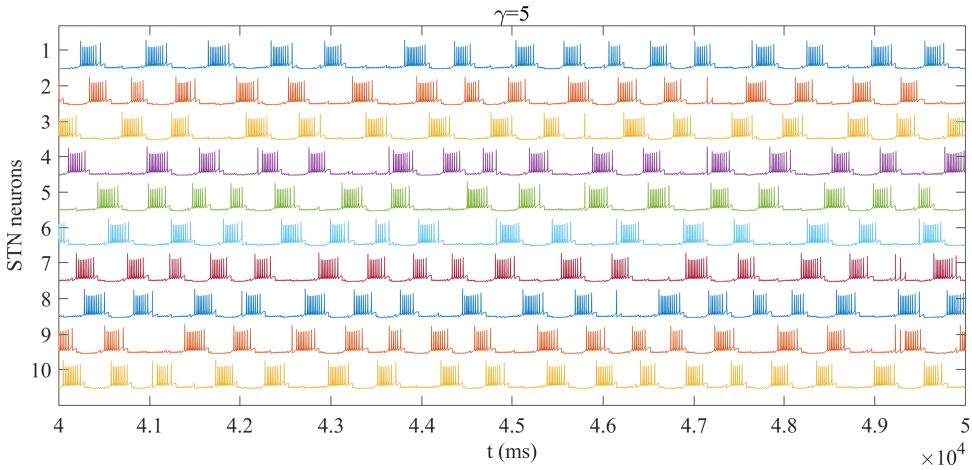

Figure 6. STN population patterns under sparsely connected when coupling strength $\gamma = 5$. It is still discharging in a continuous wave.

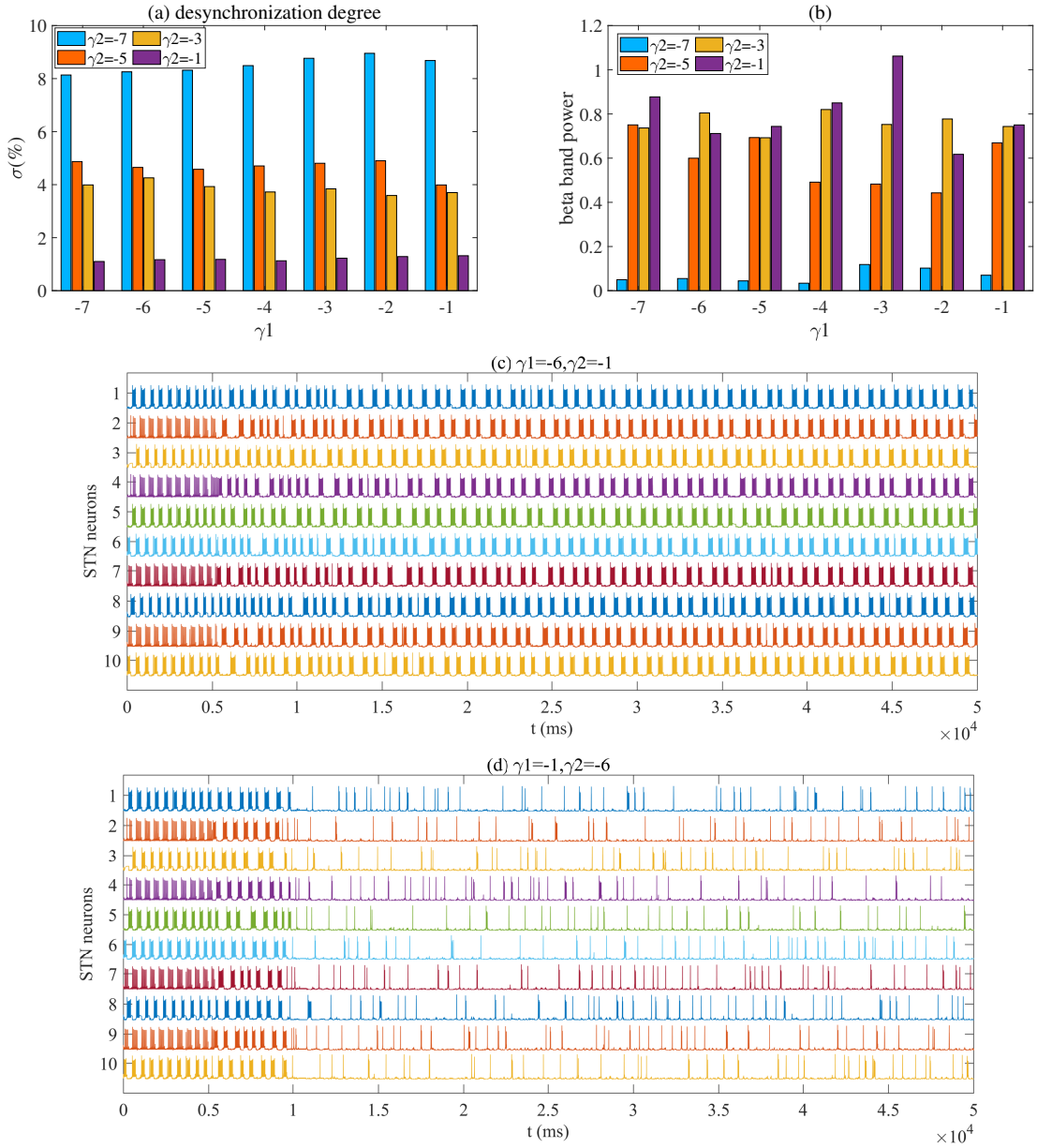

Figure 7. Degree of desynchronization (a) and beta band power (b) under different coupling strength γ_1 and γ_2. γ_2 plays a dominant role in regulating neuronal firing patterns, changing synchrony and beta oscillations. (c) $\gamma_1 = -6$, $\gamma_2 = -1$, the firing pattern do not have obvious change. (d) $\gamma_1 = -1$, $\gamma_2 = -6$, the pathological oscillation is weakend and even eliminated. Here, we add the effect of astrocytes at $t = 0.5 * 10^4$ ms.

As the coupling strength γ increases, that is, when the inhibitory effect of astrocytes on the STN and the excitatory effect on the GPe increase, we can see that the desynchronization index of the STN becomes larger and larger (shown in Figure 5(b1)), which means that the synchronized oscillations between the STN neurons become weaker and weaker; at the same time, the beta oscillation power of the STN neurons gradually recede (shown in Figure 5(b2)). Figure 5(c) shows the situation when γ is set to -2.5, the discharge mode of the STN transitions from pathological oscillation to continuous

firing. At the same time, the synchronization level among the 10 STN neurons also significantly decreases, as illustrated in Figure 5(e1), where the equal-time correlation matrix is used to measure the synchronization level:

$$C_{ij}(t_c) = \frac{1}{N} \sum_{n \in T(t_c)} [\tilde{X}_i(t_n)\tilde{X}_j(t_n)], \tag{3.3}$$

$$\tilde{X}_i(t_n) = \frac{X_i(t_n) - \overline{X}_i(t_n)}{\sigma_i}, \tag{3.4}$$

$$S = \frac{M}{M-1}[\frac{\lambda_M}{\sum_{i=1}^{M} \lambda_i} - \frac{1}{M}]. \tag{3.5}$$

The detailed explanations of all parameters can be found in [31]. Specifically, S = 1 means that all the STN neurons are completely synchronized, whereas S = 0 indicates that all STN neurons are completely out of synchronization. In addition, it should be noted that when the value of γ is small, for example, equal to -2, as shown in the Figure 5(d), the discharge pattern of the STN neurons has almost no change and is still in a continuous cluster discharge state. Figure 5(e2) shows the corresponding synchronicity change over time, in which the synchrony level is generally high. The discharge mode and synchronization of the STN do not change obviously, so we still consider it to be pathological at this case.

Furthermore, we consider the situation when γ takes a positive value, which corresponds to the excitatory effect of astrocytes on the STN and inhibitory effect on the GPe. In fact, in this case, no matter how γ changes, the initial pathological discharge state of the STN will not change significantly. As shown in Figure 6, $\gamma = 5$ is used as an example for a schematic explanation.

Finally, as displayed in Figure 7, we comprehensively consider the situation $\gamma_1 \neq \gamma_2$. Overall, when γ_2 is fixed and γ_1 varies, there is little difference in the synchrony between neurons and the power of beta oscillations. As γ_2 gradually changes from -1 to -7, no matter how γ_1 changes, the overall desynchronization index becomes larger, that is, the synchronization of neurons weakens, and at the same time, the power of beta oscillation also gradually decreases. This indicates that γ_2 plays a dominant role in regulating neuronal firing patterns, changing synchrony, and in beta oscillations. Figure 7(c),(d) show two special cases, respectively.

3.3. Tightly connected circuit without astrocytes

As described in [19], episodic and waves are the most common pathological patterns in sparsely connected neural networks. In order to obtain a more relevant rhythm, according to [19], we further consider the tightly connected coupling mode shown in Figure 8.

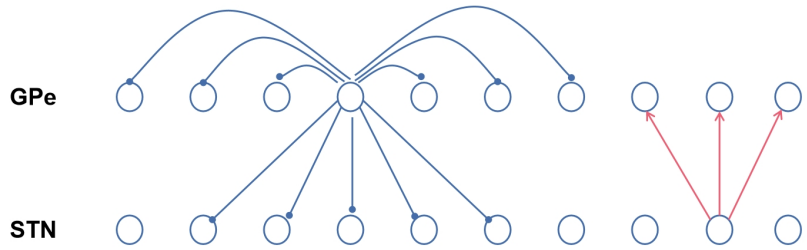

Figure 8. Schematic diagram of tightly connected circuit of 10 STN neurons and 10 GPe neurons. Each STN neuron sends excitatory input to the three closest GPe. Each GPe not only inhibits six other GPe neurons adjacent to it, but also has inhibitory connections with five STN neurons that are next to it. The blue lines represent inhibitory connections and the red lines represent excitatory connections.

Similarly, we obtain five different firing patterns at different levels of synaptic strength, as Figure 9 illustrates. Fixing $g_{GPe\to GPe} = 0.01$ and $g_{STN\to GPe} = 2$, we can obtain some discrete and irregular firings. When $g_{GPe\to STN} = 2.25$, there will be a sparse firing, as seen in Figure 9(a); decreasing $g_{GPe\to STN}$ to 1 results in weak cluster, as shown in Figure 9(b). Compared to weak cluster, if lifting $g_{GPe\to GPe}$ to 0.06, then a continuous cluster will show up, as shown in Figure 9(c). Keeping $g_{GPe\to GPe} = 0.06$, when $g_{STN\to GPe} = 0.8$ and $g_{GPe\to STN} = 3.6$, continuous wave will be produced, as seen in Figure 9(d). Strengthening $g_{STN\to GPe} = 1.3$, there will appear continuous firing pattern, as seen Figure 9(e). In the tightly connected network, continuous cluster, continuous wave, and continuous firing all exhibit obvious and highly in-phase and anti-phase discharge patterns. It is worth noting that these three firing patterns are generally regarded as abnormal activities highly correlated with PD.

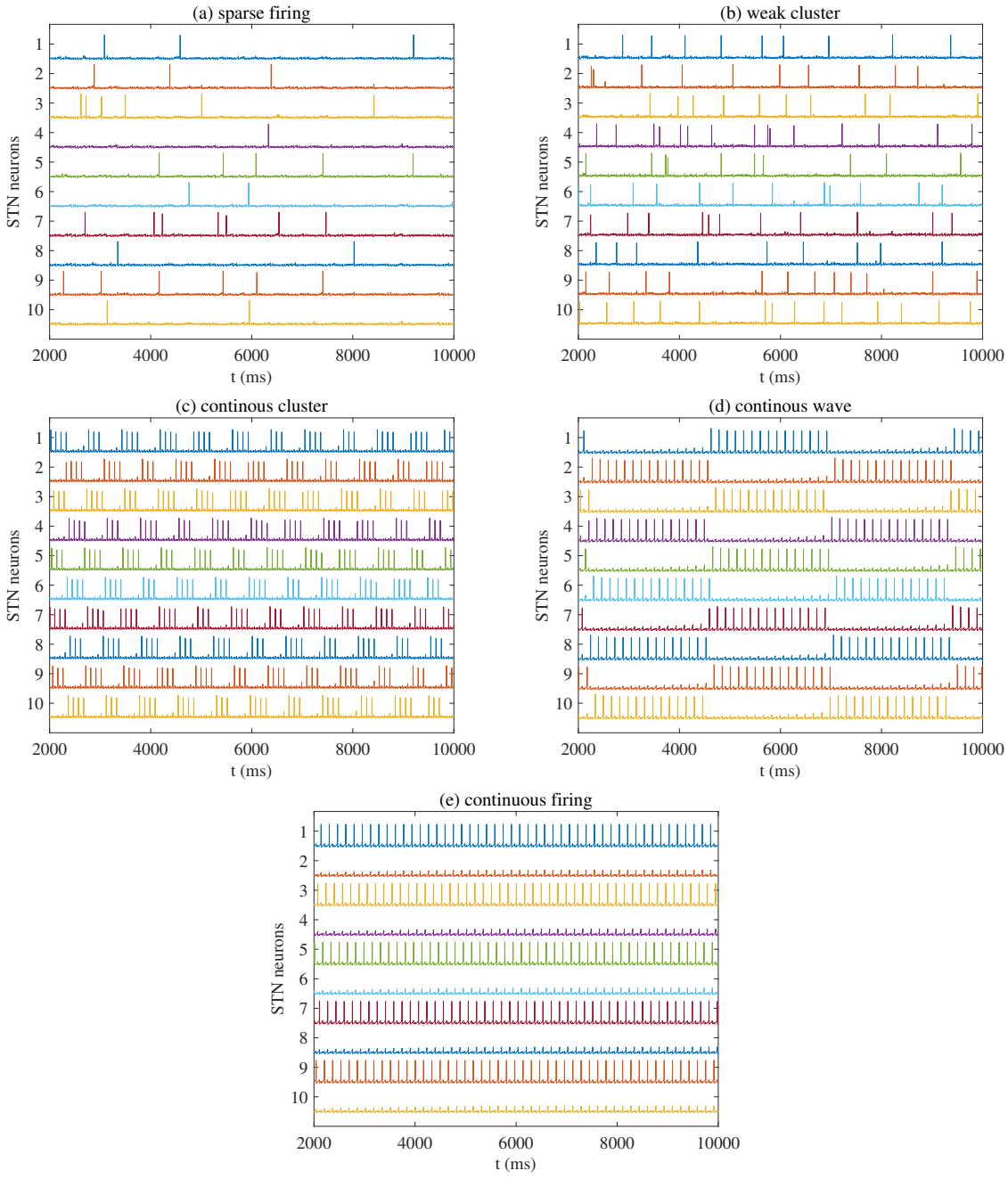

Figure 9. The activity patterns of STN neuron in the tightly connected network. Five distinct firing patterns can be obtained by varying the values of synaptic model parameters. (a) $g_{GPe\to GPe} = 0.01\ nS/\mu m^2$, $g_{STN\to GPe} = 2\ nS/\mu m^2$, $g_{GPe\to STN} = 2.25\ nS/\mu m^2$. (b) $g_{GPe\to GPe} = 0.01\ nS/\mu m^2$, $g_{STN\to GPe} = 2\ nS/\mu m^2$, $g_{GPe\to STN} = 1\ nS/\mu m^2$. (c) $g_{GPe\to GPe} = 0.06\ nS/\mu m^2$, $g_{STN\to GPe} = 2\ nS/\mu m^2$, $g_{GPe\to STN} = 1\ nS/\mu m^2$. (d) $g_{GPe\to GPe} = 0.06\ nS/\mu m^2$, $g_{STN\to GPe} = 0.8\ nS/\mu m^2$, $g_{GPe\to STN} = 3.6\ nS/\mu m^2$. (e) $g_{GPe\to GPe} = 0.06\ nS/\mu m^2$, $g_{STN\to GPe} = 1.3\ nS/\mu m^2$, $g_{GPe\to STN} = 3.6\ nS/\mu m^2$.

3.4. Tightly connected circuit with astrocytes

In the context of tight connections, we also consider the influence of astrocytes on the firing pattern of the network, where a schematic diagram of the connections is shown in the Figure 10.

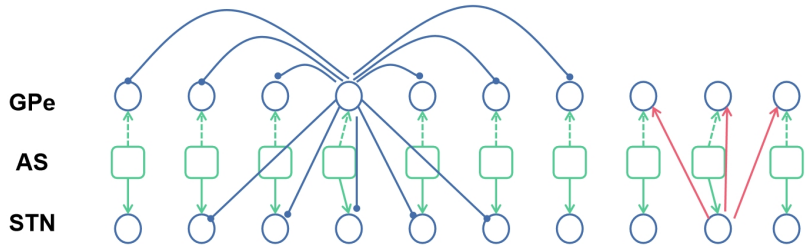

Figure 10. Schematic diagram of tightly connected circuit of STN-GPe-AS (astrocytes). The connection between STN-GPe is the same as that shown in Figure 8. Each astrocyte acts on the adjacent STN and GPe. The blue lines represent inhibitory connections and the red lines represent excitatory connections. Solid and dotted lines in green indicate the effects of astrocytes on STN and GPe respectively.

First, continuous waves are used as a background state to explore the role of astrocytes. As shown in Figure 11, when the coupling strength is varied, the firing pattern of the STN and the synchronization between neurons change correspondingly. Under a proper coupling strength, astrocytes can transfer continuous waves of background state to the other four discharge modes, holding the characteristic of non-synchronization. Furthermore, we set the value of γ from -0.7 to -2.5 (seen Figure 12), and find that the synchronization is greatly reduced within this parameter range, while the power of beta band does not drop below the level of the initial pathological state until about -1.2. Therefore, in summary, when $\gamma \in (-2.5, -1.2)$, astrocytes can achieve effective regulatory effects.

Similar to the situation of sparse connections, when γ takes a positive value, that is, astrocytes have an excitatory effect on the STN and an inhibitory effect on the GPe, no matter how γ changes, astrocytes have no significant regulatory effect on pathological discharge patterns. Figure 13 takes $\gamma = 2.5$ as an example to illustrate.

Finally, we consider the case where $\gamma_1 \neq \gamma_2$. As shown in Figure 14, when γ_2 is fixed, it can be seen that the synchronization and beta oscillation power do not significantly change as γ_1 changes. On the contrary, when γ_1 is fixed, these two indicators will change obviously with the change of γ_2, and the larger the γ_2, the greater the desynchronization index, that is, a decrease of synchronization, accompanied by a decrease of beta oscillation power. These results still indicate that γ_2 plays a leading role in the regulation of PD. This may be due to the fact that the STN is mainly subject to the inhibitory projection of the GPe, and the inhibitory effect of the GPe on the STN is weakened in PD state. Therefore, when the excitatory effect of astrocytes on the GPe is greater, the inhibitory projection of the GPe on the STN can be restored, thus regulating PD state. In addition, the results also showed that the connection mode of the STN-GPe circuit does not affect the regulation effect of astrocytes on PD.

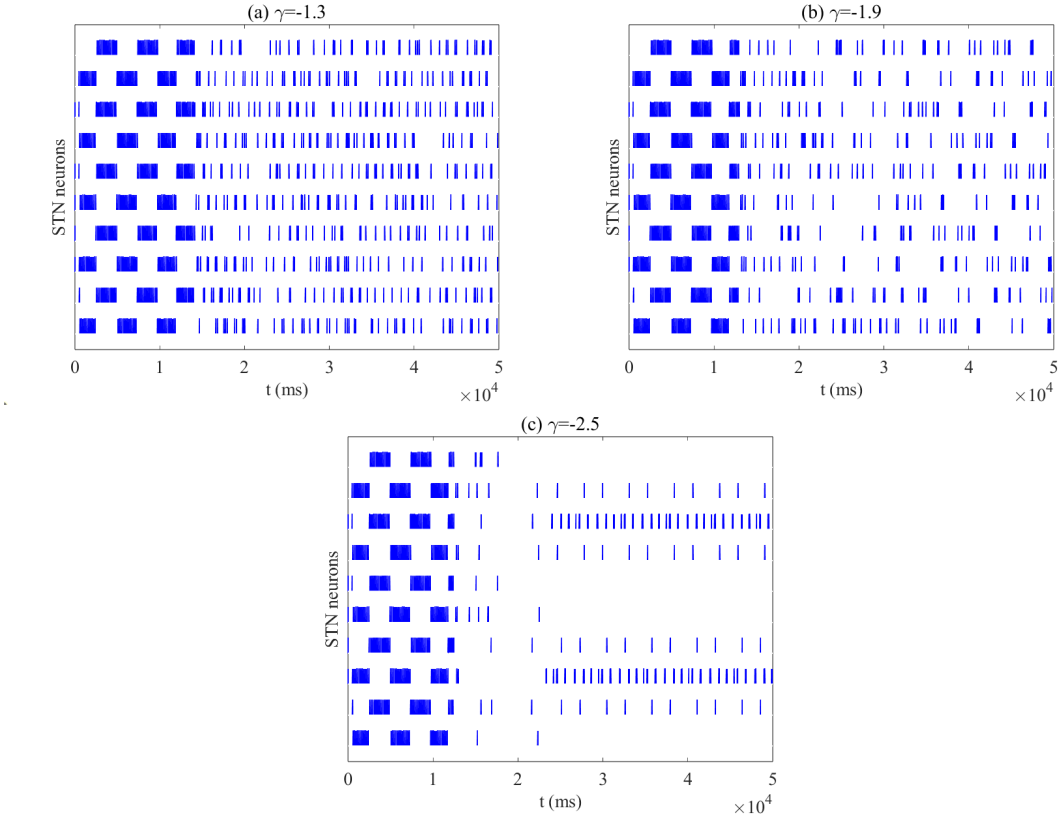

Figure 11. The response of STN population under different coupling strength γ. (a) $\gamma = -1.3$. (b) $\gamma = -1.9$. (c) $\gamma = -2.5$. The initial pathological selection of continuous waves with obvious synchronicity as shown in Figure 9(d). Under appropriate coupling strength, the continuous waves that represent the pathology can be broken or even eliminated, and the neurons will always remain out of sync in the process.

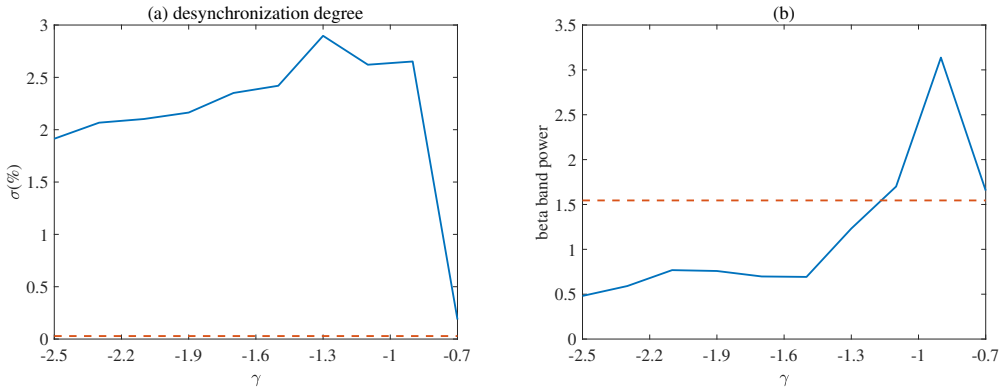

Figure 12. The relationship between the two dynamical measures (i.e., desynchronization degree (a) and the beta band power (b)) and γ. The red dotted line indicates the baseline value corresponding to the initial pathological state. When $\gamma \in (-2.5, -1.2)$, desynchronization degree stays in a high level, meaning that the synchronization is greatly reduced, and the beta oscillation is also weakend.

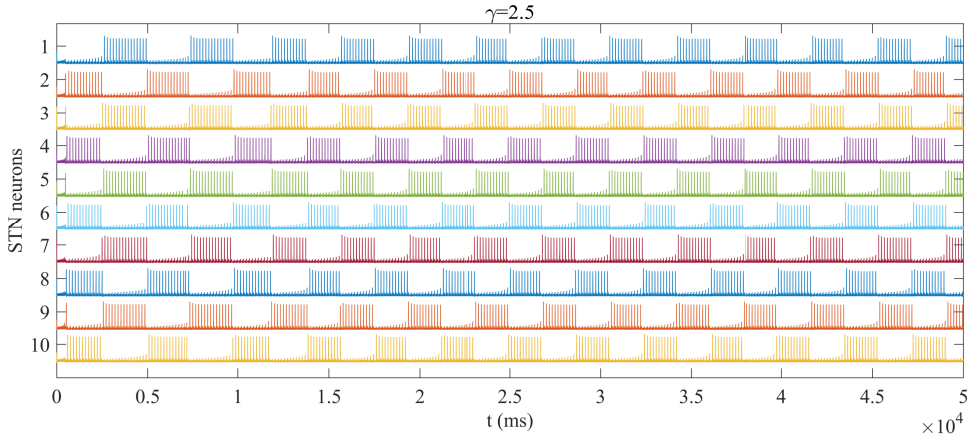

Figure 13. STN population patterns under tightly connected when coupling strength $\gamma = 2.5$. The initial pathological discharge state of the STN do not change, and still keep high synchronization.

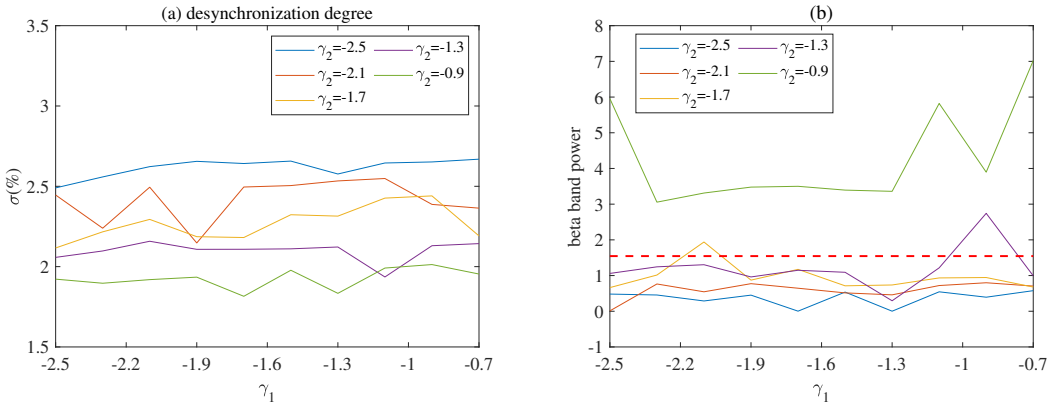

Figure 14. Degree of desynchronization (a) and beta band power (b) under different coupling strength γ_1 and γ_2. The red dotted line indicates the baseline value corresponding to the initial pathological state. γ_2 plays a dominant role in regulating neuronal firing patterns, changing synchrony and beta oscillations.

4. Conclusions and discussion

This work focused on the simulation and analysis of astrocytes on the basal ganglia network. We utilized the STN-GPe model because of its straightforward architecture that represents its crucial pacemaker role in basal ganglia [19, 29], which is highly related to the generation of PD-related firing patterns.

To begin with, we first took the sparsely connected circuit to reproduce five typical firing modes that corresponded to the severity of PD symptoms. Our study theoretically showed how astrocytes regulate neuronal excitability and thus alter their firing patterns. Specifically, the results indicated that when astrocytes inhibit the STN and excite the GPe ($\gamma \in (-2.3, -7)$), they could achieve transitions between different basic waveforms of the STN, and had certain effects on the synchrony and beta oscillations,

which meant an improvement of PD pathology. Especially when γ was greater than -5, the beta oscillation was reduced by about 70%. At the same time, the coupling strength between astrocytes and the GPe played a dominant role in the transition process. Similar results are found in the case of tight connections. Under an appropriate coupling strength ($\gamma \in (-1.3, -2.5)$), abnormal discharge modes could be destroyed, suppressed, or even eliminated, which includes the transition between different discharge patterns, the destruction of high synchronization among neurons, and the attenuation of excessive beta oscillations. It shows that the results we obtained were robust to a certain extent. The mechanism by which astrocytes exert their effect may be the compensatory effect of dopamine loss, that is, astrocytes compensate for the action of the missing dopamine transmitter to a certain extent, thus affecting the STN-GPe circuit. All these results suggest that astrocytes may be a promising new therapeutic target for PD.

However, this study simplified the modeling process, making it easier to process and analyze, but at the same time inevitably had some assumptions and limitations. The first is the simplification of network size, where the limited number of neurons in the model might not have been enough to fully capture the complexity of large neural networks, especially when it came to multi-regional interactions. Additionally, the model only considered the STN and the GPe, and ignored neurons in other basal ganglia structures, such as the Globus pallidus internus (GPi) and substantia nigra dopaminergic neurons, which also play a key role in PD. Second, this work was only a preliminary exploration of the effect of the connections between astrocytes and neurons on PD; therefore, it did not consider the connections between astrocytes. In addition, the modeling of astrocytes was simplified and only the key features of astrocyte calcium oscillation were considered. Therefore, in order to more accurately simulate the complex dynamics of the brain in future modeling studies, more refined models are needed, including more cell types, more detailed synaptic dynamics, and more precise anatomical connectivity.

Use of AI tools declaration

The authors declare they have not used Artificial Intelligence (AI) tools in the creation of this article.

Acknowledgments

This research was supported by the National Natural Science Foundation of China (Nos. 12072265, 12372064).

Conflict of interest

The authors declare there is no conflict of interest.

References

1. S. Mullin, A. H. V. Schapira, Pathogenic mechanisms of neurodegeneration in Parkinson disease, *Neurol. Clin.*, **33** (2015), 1–17. https://doi.org/10.1016/j.ncl.2014.09.010
2. A. Galvan, A. Devergnas, T. Wichmann, Alterations in neuronal activity in basal ganglia-thalamocortical circuits in the parkinsonian state, *Front. Neuroanat.*, **9** (2015), 5. https://doi.org/10.3389/fnana.2015.00005

3. P. Silberstein, A. KuÈhn, A. Kupsch, T. Trottenberg, J. Krauss, J. WoÈhrle, et al., Patterning of globus pallidus local field potentials differs between Parkinson's disease and dystonia, *Brain*, **126** (2003), 2597–2608. https://doi.org/10.1093/brain/awg267

4. S. Kim, E. Pajarillo, I. Nyarko-Danquah, M. Aschner, E. Lee, Role of astrocytes in Parkinson's disease associated with genetic mutations and neurotoxicants, *Cells*, **12** (2023), 622. https://doi.org/10.3390/cells12040622

5. L. Iovino, M. E. Tremblay, L. Civiero, Glutamate-induced excitotoxicity in Parkinson's disease: the role of glial cells, *J. Pharmacol. Sci.*, **144** (2020), 151–164. https://doi.org/10.1016/j.jphs.2020.07.011

6. H. Kwon, S. Koh, Neuroinflammation in neurodegenerative disorders: the roles of microglia and astrocytes, *Transl. Neurodegener.*, **9** (2020), 42. https://doi.org/10.1186/s40035-020-00221-2

7. H. D. E. Booth, W. D. Hirst, R. Wade-Martins, The role of astrocyte dysfunction in Parkinson's disease pathogenesis, *Trends Neurosci.*, **40** (2017), 358–370. https://doi.org/10.1016/j.tins.2017.04.001

8. W. Chung, N. J. Allen, C. Eroglu, Astrocytes control synapse formation, function, and elimination, *Cold Spring Harbor Perspect. Biol.*, **7** (2015), a020370. https://doi.org/10.1101/cshperspect.a020370

9. I. Miyazaki, M. Asanuma, Neuron-astrocyte interactions in Parkinson's disease, *Cells*, **9** (2020), 2623. https://doi.org/10.3390/cells9122623

10. N. Mallet, L. Delgado, M. Chazalon, C. Miguelez, J. Baufreton, Cellular and synaptic dysfunctions in Parkinson's disease: stepping out of the striatum, *Cells*, **8** (2019), 1005. https://doi.org/10.3390/cells8091005

11. J. Giehrl-Schwab, F. Giesert, B. Rauser, C. L. Lao, S. Hembach, S. Lefort, et al., Parkinson's disease motor symptoms rescue by CRISPRa-reprogramming astrocytes into GABAergic neurons, *EMBO Mol. Med.*, **14** (2022), e14797. https://doi.org/10.15252/emmm.202114797

12. K. Chen, H. Wang, I. Ilyas, A. Mahmood, L. Hou, Microglia and astrocytes dysfunction and key neuroinflammation-based biomarkers in Parkinson's disease, *Brain Sci.*, **13** (2023), 634. https://doi.org/10.3390/brainsci13040634

13. A. N. Brandebura, A. Paumier, T. S. Onur, N. J. Allen, Astrocyte contribution to dysfunction, risk and progression in neurodegenerative disorders, *Nat. Rev. Neurosci.*, **24** (2023), 23–39. https://doi.org/10.1038/s41583-022-00641-1

14. V. Volman, M. Bazhenov, T. J. Sejnowski, Computational models of neuron-astrocyte interaction in epilepsy, *Front. Comput. Neurosci.*, **6** (2012), 58. https://doi.org/10.3389/fncom.2012.00058

15. J. Tang, J. Zhang, J. Ma, G. Zhang, X. Yang, Astrocyte calcium wave induces seizure-like behavior in neuron network, *Sci. China Technol. Sci.*, **60** (2017), 1011–1018. https://doi.org/10.1007/s11431-016-0293-9

16. D. A. Iacobas, S. O. Suadicani, D. C. Spray, E. Scemes, A stochastic two-dimensional model of intercellular Ca2+ wave spread in glia, *Biophys. J.*, **90** (2006), 24–41. https://doi.org/10.1529/biophysj.105.064378

17. A. N. Silchenko, P. A. Tass, Computational modeling of paroxysmal depolarization shifts in neurons induced by the glutamate release from astrocytes, *Biol. Cybern.*, **98** (2008), 61–74. https://doi.org/10.1007/s00422-007-0196-7

18. D. Reato, M. Cammarota, L. C. Parra, G. Carmignoto, Computational model of neuron-astrocyte interactions during focal seizure generation, *Front. Comput. Neurosci.*, **6** (2012), 81. https://doi.org/10.3389/fncom.2012.00081

19. D. Terman, J. E. Rubin, A. C. Yew, C. J. Wilson, Activity patterns in a model for the subthalamopallidal network of the basal ganglia, *J. Neurosci.*, **22** (2002), 2963–2976. https://doi.org/10.1523/JNEUROSCI.22-07-02963.2002

20. J. E. Rubin, D. Terman, High frequency stimulation of the subthalamic nucleus eliminates pathological thalamic rhythmicity in a computational model, *J. Comput. Neurosci.*, **16** (2004), 211–235. https://doi.org/10.1023/B:JCNS.0000025686.47117.67

21. J. Best, C. Park, D. Terman, C. Wilson, Transitions between irregular and rhythmic firing patterns in excitatory-inhibitory neuronal networks, *J. Comput. Neurosci.*, **23** (2007), 217–235. https://doi.org/10.1007/s10827-007-0029-7

22. V. Volman, E. Ben-Jacob, H. Levine, The astrocyte as a gatekeeper of synaptic information transfer, *Neural Comput.*, **19** (2007), 303–326. https://doi.org/10.1162/neco.2007.19.2.303

23. Z. Ouyang, Y. Yu, Z. Liu, P. Feng, Transition of spatiotemporal patterns in neuron–astrocyte networks, *Chaos, Solitons Fractals*, **169** (2023), 113222. https://doi.org/10.1016/j.chaos.2023.113222

24. J. Zhao, D. Fan, Q. Wang, Q. Wang, Dynamical transitions of the coupled class I (II) neurons regulated by an astrocyte, *Nonlinear Dyn.*, **103** (2021), 913–924. https://doi.org/10.1007/s11071-020-06122-3

25. M. Amiri, F. Bahrami, M. Janahmadi, Functional contributions of astrocytes in synchronization of a neuronal network model, *J. Theor. Biol.*, **292** (2012), 60–70. https://doi.org/10.1016/j.jtbi.2011.09.013

26. M. Amiri, N. Hosseinmardi, F. Bahrami, M. Janahmadi, Astrocyte-neuron interaction as a mechanism responsible for generation of neural synchrony: a study based on modeling and experiments, *J. Comput. Neurosci.*, **34** (2013), 489–504. https://doi.org/10.1007/s10827-012-0432-6

27. J. J. Wade, L. J. McDaid, J. Harkin, V. Crunelli, J. A. S. Kelso, Bidirectional coupling between astrocytes and neurons mediates learning and dynamic coordination in the brain: a multiple modeling approach, *PLOS One*, **6** (2011), e29445. https://doi.org/10.1371/journal.pone.0029445

28. D. Fan, Q. Wang, Improving desynchronization of parkinsonian neuronal network via triplet-structure coordinated reset stimulation, *J. Theor. Biol.*, **370** (2015), 157–170. https://doi.org/10.1016/j.jtbi.2015.01.040

29. H. Zhang, Y. Yu, Z. Deng, Q. Wang, Activity pattern analysis of the subthalamopallidal network under ChannelRhodopsin-2 and Halorhodopsin photocurrent control, *Chaos, Solitons Fractals*, **138** (2020), 109963. https://doi.org/10.1016/j.chaos.2020.109963

30. Z. Cao, L. Du, H. Zhang, Y. Zhao, Z. Shen, Z. Deng, Pattern transition and regulation in a subthalamopallidal network under electromagnetic effect, *Chin. Phys. B*, **31** (2022), 118701. https://doi.org/10.1088/1674-1056/ac80ae

31. H. Zhang, J. Su, Q. Wang, Y. Liu, L. Good, J. M. Pascual, Predicting seizure by modeling synaptic plasticity based on EEG signals-a case study of inherited epilepsy, *Commun. Nonlinear Sci. Numer. Simul.*, **56** (2018), 330–343. https://doi.org/10.1016/j.cnsns.2017.08.020

AIMS Press